Supplement

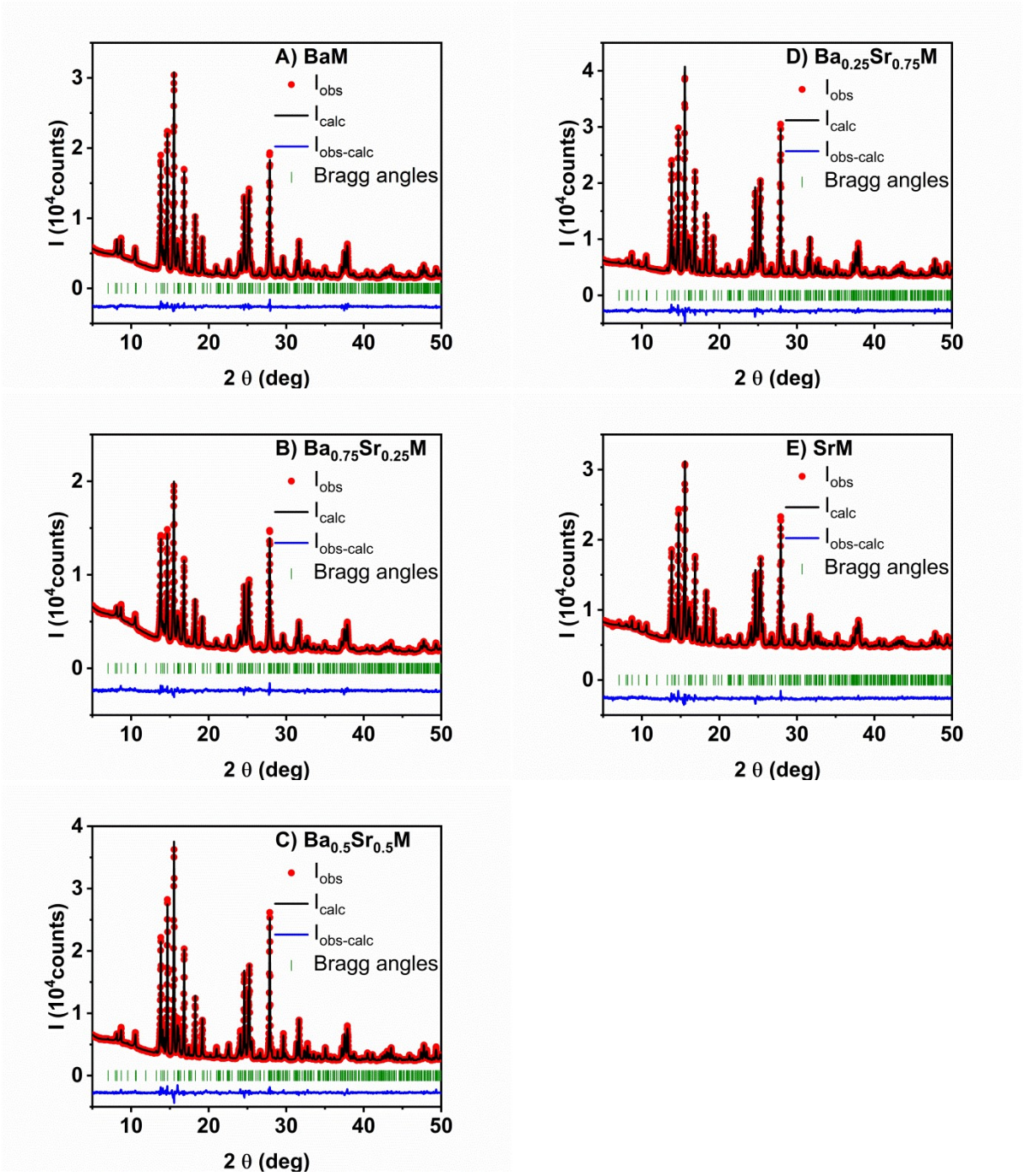

Figure (A) – (E) XRD patterns and Rietveld refinements for $Ba_{1-x}Sr_xFe_{12}O_{19}$ with x = 0, 0.25, 0.5, 0.75, 1

Table I: XRD and XRF results

x	a/*Å*	c/*Å*	V/*Å³*	ρ/*g·cm⁻³*	wR/*%*	GOF	***x* (RV)***	***x* (SC)***	***x*(XRF)***	**σ(*x*)****
0	5.8847	23.1618	694.63	5.31	2.84	1.57	**0**	**0**	**0**	**0**
0.25	5.8846	23.1466	694.15	5.25	2.68	1.51	**0.29**	**0.17**	**0.16**	**0.07**
0.5	5.8842	23.1196	693.23	5.22	2.68	1.70	**0.45**	**0.4**	**0.39**	**0.09**
0.75	5.8810	23.0730	691.09	5.16	2.44	1.72	**0.77**	**0.65**	**0.65**	**0.08**
1	5.8769	23.0180	688.49	5.12	1.81	1.42	**1**	**1**	**0.99**	**0**

* Ba/Sr-ratio from Rietveld refinements (RV), single crystal data (SC) and X-ray fuorescence data (XRF)

** σ(*x*) is the standard deviation calculated from the *x* values of the three methods compared to nominal *x*

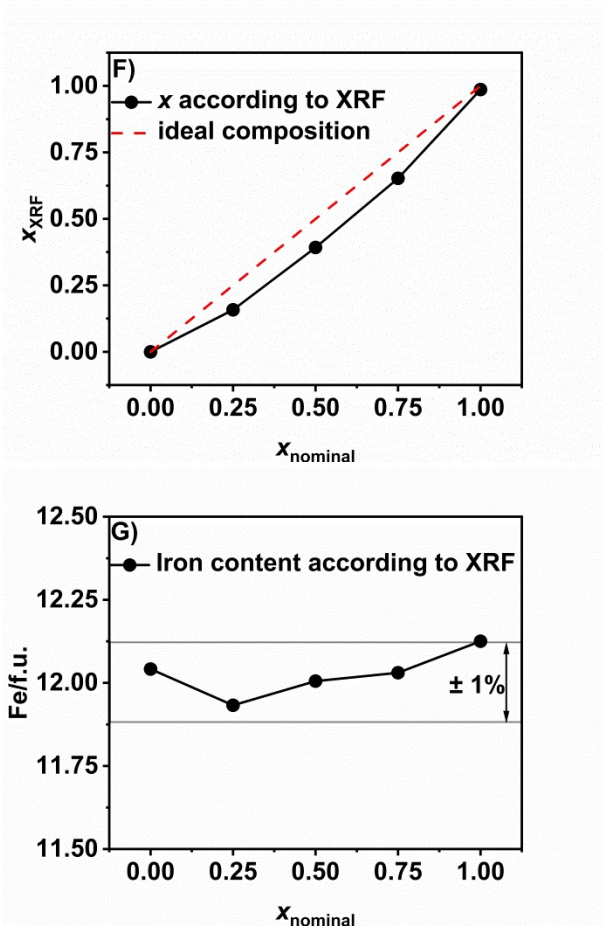

Figure (F) Sr-content per formula unit and number of Fe^{3+} per formula unit (G) determined by X-ray fluorescence spectroscopy

The Ba/Sr-stoichiometry and iron content were additionally checked via X-ray fluorescence analysis. Figure (F) and (G) show that *x* and the number of ferric ions per formula unit are in good accordance with the expected stoichiometry.

Figure (H) shows the hysteresis of the SrM single crystal at 5 *K* measured with B || <100>. The negligibly low values of remanence and coercivity in combination with the linear increase of μ with B up to saturation indicate reversible soft magnetization behaviour. For this reason, additional contributions arising from domain-domain interactions, preferred domain growth directions and other phenomena can be neglected and one can assume that the energy of the external field is solely used to align the magnetic moment of the sample either by rotation of a single magnetic crystal moment μ_S or via a shifting of domain walls through the crystal without any perceptible resistance. The work required for aligning a magnetic moment parallel to an external field is $W = \vec{m} \cdot \vec{B}$. As the remanence is close to zero and μ increases linearly with B, a good approximation for W is to use half of the area of the rectangle given by μ_S and B_S, i.e. $W = \frac{1}{2}\mu_S \cdot B_S$ as shown in the right upper quadrant of Figure (H). The value of B_s can be derived from the intersection of the two tangents of the $\mu \propto B$ and the $\mu = const.$ regions as shown in the figure. In addition, the magnetization energies were also calculated by a 'pseudo-Lebesgue integration', i.e. a numerical integration as shown in the lower left quadrant of Figure (H). We found that the energies calculated by the two approaches differ by only a few percent. Nevertheless, the more precise values from the pseudo-

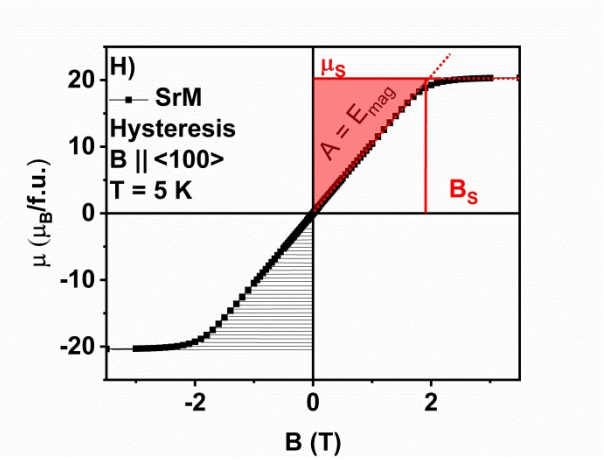

Figure (H) Principle of calculating the magnetization energies from a hysteresis graph

Lebesgue integration were used in the discussion.

Table II: Results of single crystal structure refinements

	Wyckoff	**x/*a***	**y/*b***	**z/*c***	**SOF***	
Ba/Sr	2 *d*	2/3	1/3	1/4	$\Sigma_{Ba+Sr} = 1$	
Fe1	2 *a*	0	0	0	1	
Fe2	4 *e*	0	0	z	1/2	
Fe3	4 *f*	1/3	2/3	z	1	
Fe4	4 *f*	1/3	2/3	z	1	
Fe5	12 *k*	x	2 x	z	1	
O1	4 *e*	0	0	z	1	
O2	4 *f*	1/3	2/3	z	1	
O3	6 *h*	x	2x	1/4	1	
O4	12 *k*	x	2x	z	1	
O5	12 *k*	x	2x	z	1	
	***x* (Sr/f.u.)**	**0**	**0.25**	**0.5**	**0.75**	**1**
Ba/Sr	SOF* (Sr)	0	0.17	0.4	0.65	1
	$U_{iso}/Å^2$	0.0045(2)	0.00361(19)	0.00642(18)	0.0068(2)	0.0086(3)
Fe1	$U_{iso}/Å^2$	0.0027(3)	0.0016(3)	0.0038(2)	0.0025(2)	0.0018(3)
Fe2	z/*c*	0.25727(9)	0.25726(8)	0.25709(8)	0.2565(3)	0.2558(5)
	$U_{iso}/Å^2$	0.0033(4)	0.0009(3)	0.0024(3)	0.0017(12)	0.0018(14)
Fe3	z/*c*	0.02719(5)	0.02721(4)	0.02724(4)	0.02730(4)	0.02724(5)
	$U_{iso}/Å^2$	0.0028(3)	0.0014(2)	0.0034(2)	0.0023(2)	0.0010(2)
Fe4	z/*c*	0.19030(5)	0.19045(5)	0.19050(4)	0.19066(4)	0.19091(5)
	$U_{iso}/Å^2$	0.0030(3)	0.0014(2)	0.0034(2)	0.0026(2)	0.0018(2)
Fe5	x/*a*	0.16878(7)	0.16873(5)	0.16878(5)	0.16878(5)	0.16871(5)
	z/*c*	0.89180(3)	0.89163(3)	0.89144(2)	0.89112(2)	0.89075(3)
	$U_{iso}/Å^2$	0.0030(2)	0.00164(19)	0.00353(17)	0.0027(2)	0.0020(2)
O1	z/c	0.1506(3)	0.1505(2)	0.1506(2)	0.1508(2)	0.1514(2)
	$U_{iso}/Å^2$	0.0045(9)	0.0026(7)	0.0044(7)	0.0022(7)	0.0015(7)
O2	z/*c*	-0.0544(3)	-0.0542(2)	-0.0546(2)	-0.0549(2)	-0.0548(2)
	$U_{iso}/Å^2$	0.0043(10)	0.0022(8)	0.0042(8)	0.0036(7)	0.0028(8)
O3	x/*a*	0.1829(6)	0.1827(4)	0.1822(4)	0.1824(4)	0.1825(4)
	$U_{iso}/Å^2$	0.0074(9)	0.0048(7)	0.0074(7)	0.0060(7)	0.0066(8)
O4	x/*a*	0.1561(3)	0.1563(3)	0.1563(3)	0.1564(2)	0.1561(3)
	z/*c*	0.05197(16)	0.05217(14)	0.05221(13)	0.05227(13)	0.05247(16)
	$U_{iso}/Å^2$	0.0041(6)	0.0024(5)	0.0046(5)	0.0031(4)	0.0024(5)
O5	x/*a*	0.5021(3)	0.5027(3)	0.5031(3)	0.5038(2)	0.5046(3)
	z/*c*	0.14962(16)	0.15003(13)	0.15017(12)	0.15064(12)	0.15109(15)
	$U_{iso}/Å^2$	0.0037(6)	0.0027(5)	0.0051(5)	0.0039(4)	0.0037(5)
	a/*Å*	5.8998(8)	5.8956(8)	5.8915(8)	5.8955(8)	5.8896(8)
	c/*Å*	23.259(5)	23.224(5)	23.155(5)	23.100(5)	23.100(5)
	V/ $Å^3$	701.1(2)	699.08(19)	696.04(19)	695.32(19)	693.92(19)
		-9< h <+8	-8< h <+6	-9< h <+9	-7< h <+9	-9< h <+9
	hkl-range	-9 < k <+3	-8< k <+9	-6< k <+9	-9< k <+9	-9< k <+8
		-27< l <+36	-36< l <+18	-24< l <+36	-27< l <+36	-36< l <+14
	R_1	0.0628	0.0495	0.0449	0.0442	0.0544
	wR_2	0.1426	0.1169	0.1069	0.1193	0.1297
	GooF	1.336	1.348	1.340	1.449	1.229

* SOFs of Ba/Sr were refined for mixed compounds; SOFs of Fe and O were fixed to 1 because their refinements led to values close to unity